Transport in Porous Media (2023) 149:479–499
https://doi.org/10.1007/s11242-023-01962-0

Water Harvesting by Molecular Sieves Using Self-sustained Continuous Flow

Ulises Torres-Herrera[1] · **María Fernanda Ballesteros-Rivas**[1,2] · **Víctor Varela-Guerrero**[1,2] · **Jorge Balmaseda**[3]

Received: 7 June 2022 / Accepted: 12 May 2023 / Published online: 5 June 2023

Abstract

A way of harvesting water from the air that avoids the discontinuity of the adsorption/desorption cycles is theoretically analyzed. A rectangular prism-shaped adsorbent bed is immersed in low-humidity air, at an angle to the horizontal and subject to a temperature gradient between two opposite and open faces. The other four faces of the prism remain isolated. Water is adsorbed on the adsorbent colder face, causing a density gradient in the surrounding air, parallel to the surface, that results in a self-sustained continuous air flow. On the opposite face, a self-sustained continuous air flow parallel to the surface also arises, but this time due to a temperature gradient in the air surrounding the hot bed face. In addition, its higher temperature causes the desorption of water from the adsorbent. This overall water exchange produces the enrichment of water content in one of the air streams that is crucial to produce water harvesting. The performance of Al-Fumarate, MOF-303, SAPO-34 and Zeolite 13X is tested, unveiling the key factors that increase flow rate and water concentration at the enriched phase. It has been found that the diffusive mass transport at the air-solid interphase is the bottleneck of water harvesting in continuous flow conditions. Therefore, if high concentration of water is desired, it is necessary to use porous materials with very high diffusitivities. These findings provide the foundations for the design of continuous water harvesting devices.

Article Highlights

- The performance of four molecular sieves with enhanced water adsorption properties is tested for continuous harvesting.

✉ Ulises Torres-Herrera
torres.herrera.ulises@hotmail.com

✉ Jorge Balmaseda
balmaseda@comunidad.unam.mx

[1] Facultad de Química, Universidad Autónoma del Estado de México, Paseo Colón S/N, 50120 Toluca de Lerdo, Mexico

[2] Centro Conjunto de Investigación en Química Sustentable, UAEM-UNAM, Carr. Toluca-Atlacomulco Km 14.5, 50200 Toluca de Lerdo, Mexico

[3] Departamento de Polímeros, Instituto de Investigaciones en Materiales, Universidad Nacional Autónoma de México, 04510 Mexico City, Mexico

- A theoretical model is done by coupling natural air convection with non-fickean water transport inside molecular sieves.
- High diffusion coefficient of water in porous media plays a key role for efficient continuous water harvesting.

Keywords Molecular sieves · Natural convection · Water harvesting · Zeolites · Metal–organic framework · Self-sustained continuous flow

List of Symbols

β	Isobaric thermal expansion coefficient, K^{-1}
β_w	Isobaric humidity expansion coefficient, $kg^{-1}\ m^3$
χ_c	Relative change of water concentration at the cold air phase, dimensionless
χ_h	Relative change of water concentration at the hot air phase, dimensionless
$\hat{C}_p$	Specific heat capacity, $J\ kg^{-1}\ K^{-1}$
c_w^s	Water concentration in the adsorbent bed, $kg\ m^{-3}$
d	Adsorbent bed thickness, m
D_0	Infinite dilution diffusion coefficient, $m^2\ s^{-1}$
$D_{w,air}$	Water diffusivity in air, $m^2\ s^{-1}$
$D_{w,s}$	Transport diffusivity of water through the solid, $m^2\ s^{-1}$
Q_{air}^c	Mass flow rate of cold air phase at the final portion of bed, $kg\ s^{-1}$
Q_{air}^h	Mass flow rate of hot air phase at the final portion of bed, $kg\ s^{-1}$
Q_w^c	Mass flow rate of water in cold air phase at the final portion of bed, $kg\ s^{-1}$
Q_w^h	Mass flow rate of water in hot air phase at the final portion of bed, $kg\ s^{-1}$
g	Free-fall acceleration, $m\ s^{-2}$
k	Air thermal conductivity, $J\ m^{-1}\ s^{-1}\ K^{-1}$
k_s	Solid thermal conductivity, $J\ m^{-1}\ s^{-1}\ K^{-1}$
L	Adsorbent bed length, m
M_{dry}	Molar mass of dry air, $kg\ mol^{-1}$
μ	Air viscosity, Pa s
M_w	Molar mass of water, $kg\ mol^{-1}$
p	Air pressure, Pa
p_{dry}	Partial pressure of dry air, Pa
p_w^{air}	Partial pressure of water in the air phases, Pa
p_w^s	Adsorption isotherm equilibrium pressure, Pa
R	Universal gas constant, $J\ mol^{-1}\ K^{-1}$
ρ_0	Atmospheric air density away from the solid surface, $kg\ m^{-3}$
ρ	Air density near the solid surface, $kg\ m^{-3}$
ρ_{w0}	Density of water in air away from the solid surface, $kg\ m^{-3}$
ρ_w^c	Density of water in the air near the cold surface, $kg\ m^{-3}$
ρ_w^h	Density of water in the air near the hot surface, $kg\ m^{-3}$
T	Temperature of solid material, K
T_0	Room temperature, K
T_1	Hot surface temperature, K
T^h	Temperature of air close to the heated surface, K
θ	Angle of inclination of the entire system respect to the horizontal, degrees
v_x^c	x-component of air velocity near the cold surface, $m\ s^{-1}$
v_x^h	x-component of air velocity near the hot surface, $m\ s^{-1}$

v_y^c y-component of air velocity near the cold surface, m s^{-1}
v_y^h y-component of air velocity near the hot surface, m s^{-1}
x Coordinate parallel to the length of the adsorbent bed, m, with zero value at the left end of the bed (see Fig. 1)
y Coordinate parallel to the thickness of the adsorbent bed, m, with zero value at the center of the bed (see Fig. 1)

Abbreviations

MOF Metal–organic framework
SAPO Silicoaluminophosphate
SEM Scanning electron microscopy

1 Introduction

Multiple sustainable development goals of United Nations rely on a common challenge: the availability of clean water. The atmosphere contains about thirteen trillion tons of water (Gleick 1998); nonetheless, water harvesting is more expensive than collecting rainwater, desalination, or remediation of wastewater and polluted water (Zhou et al. 2020). With global warming, desert regions without access to some kind of water sources have expanded. Under these conditions, water harvesting from the air becomes the only viable short-term option while more effective but long-term environmental remediation measures such as reforestation are taken. Efficient capture of water from the air is a major technological challenge due to the complexity of the gas mixture in the air and the high energy cost of the process of concentrating and condensing atmospheric water vapour (Zhou et al. 2020; Eslamian and Eslamian 2021). This has inspired the development of novel devices that use materials with specific tunable properties (Fathieh et al. 2018; Pan et al. 2020; Sakthivadivel and Vennila 2021; Levy and Eslamian 2021; Adeaga and Eslamian 2021; Kabo-Bah et al. 2021).

Air drying and water harvesting using desiccants are very similar processes. The main difference between them is that the former is used when the relative humidity is close to 100% and the latter is useful for relative humidities below 10%. However, desiccant air dryers work continuously, while water harvesting with adsorbents is done discontinuously by alternating adsorption and desorption cycles. The difference in working relative

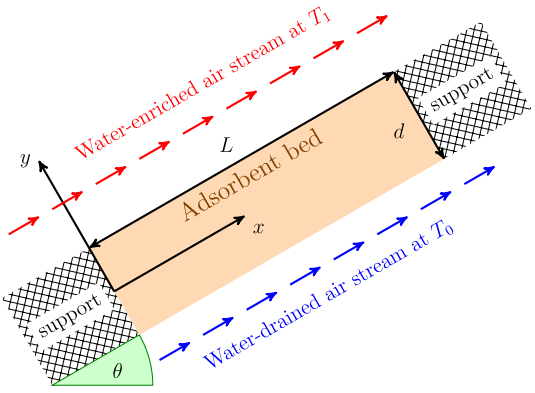

Fig. 1 Diagram of the system under study. It consists of a porous adsorbent bed in an inclined support. Since the top surface of the solid phase is subjected to a higher temperature than the surroundings, the temperature gradient induces a fluid flow by natural convection

humidity prevents desiccants used in air drying from being suitable for water harvesting. Recently, the design, development and testing of novel suitable materials for water recovery has demanded the search of molecular solid structures that combine selectivity in water capture and a simple switching from adsorption to desorption under controlled conditions, which should be easily attainable within a laboratory, a plant or, in some conditions, in field tests where the recovery of atmospheric water is desired (Trapani et al. 2016; Kim et al. 2017; Mancuso and Hendon 2019). In this direction, the design and synthesis of efficient materials has been successful because their structure includes pores that change its size and chemical interactions in response to the contact with water isolated molecules or small clusters, whereas other novel materials are capable of changing the local structure of pores at different temperatures (Nguyen et al. 2020; Zhou et al. 2020), enabling a fine tuning of the physical conditions where adsorption/desorption transition occurs (Mouchaham et al. 2020; Kim et al. 2020; Hanikel et al. 2021).

The enhanced properties of these materials can be exploited for water harvesting, when a process involving two separate stages is carried out (Kim et al. 2018; LaPotin et al. 2019). First, in the uptake stage, the initially empty porous material is surrounded by a low water concentration environment; given the excellent adsorptive capabilities of the material under such conditions, this material concentrates water efficiently until it reaches its saturation point, even when air has a very low water content (Kalmutzki et al. 2018). Afterward, the water-saturated material is moved to the water recovery place and is subject to other conditions, typically high temperatures, which modify the properties of the material, producing water desorption and its subsequent recovery, leaving the material dehydrated and ready to repeat the whole cycle again.

The above-described cycle has been successfully employed to recover water from low-concentration environments (Hanikel et al. 2019). Nonetheless, this strategy conveys intrinsic difficulties. First, the transition from adsorption to desorption stages at every cycle results in considerable energetic expenses for heating and cooling the material alternately. Then, the change from one stage to the next takes considerable time, which implies long time lapses where water recovery is interrupted during the operation. Finally, the most important challenge relies on the exhaustion that occurs in the material when it is subjected to multiple adsorption/desorption cycles, which causes that, after a short time, the material reduces its performance and must be replaced or recovered by a chemical treatment. This increases considerably the operation costs of the entire water-harvesting process and demands a constant supply of fresh porous material. These challenges have motivated the search for materials with an enhanced resistance to hydrolysis reactions that compromise the long-term durability of materials under multiple cycles of adsorption/desorption (Xu and Yaghi 2020; Öhrström and Amombo Noa 2021; Hanikel et al. 2019, 2021; Wang and Lee 2021).

The development of novel materials is a problem that involves both experimentalists and theorists in an integrated effort to design and simulate potentially useful materials for their subsequent preparation and performance testing under the conditions of the target applications. Besides to all these efforts, it is necessary to develop alternative approaches to exploit the enhanced properties of materials for water retention and release. Moving from a discontinuous to a continuous process of water harvesting would reduce costs in the creation and maintenance of storage infrastructure and allow for more compact systems. It would also provide a steady water supply. However, it is necessary to know the water harvesting capacity of these systems and the energy cost of such processes. For these reasons, an alternative to batch operation is to implement continuous-flow operation schemes, i.e., to exert specific conditions on the material such as adsorption and desorption occur

at different portions of the material simultaneously. To achieve this, the material must be subjected, at least, to two simultaneous conditions: one portion of the material needs to be under conditions that promote water adsorption, whereas another portion of the material must be under conditions that promote water desorption.

The development of continuous flow systems for simultaneous adsorption/desorption demands a change of paradigm, i.e., to reassess the desirable material properties in order to achieve optimal water recovery. It is necessary to understand and simulate in more detail the actual physical and chemical mechanisms of adsorption in novel materials, without the limitations of approximated statistical models. Moreover, it is fundamental to give insights into the emerging issues involved in continuous flow systems, in comparison with the widely known challenges of water harvesting in batch operation.

In order to exploit the properties of porous media for continuous flow systems, a vast range of theoretical and experimental results have shed light onto the physics of gases transport through porous media, both involving the adsorption and surface diffusion, along with pressure-driven convective flow (Gilliand et al. 1962; Horiguchi et al. 1971; Ash et al. 1993; Yamasaki et al. 1996). In such direction, the role of geometric properties of the particles network within porous media, along with the gas/solid interaction has been fundamental for the better understanding of desiccant performance, to some extent. Nonetheless, the statistical mechanics models relied on the assumption of weak gas/solid and gas/gas interaction within the solid phase (Hwang and Kammermeyer 1966; Gilliland et al. 1974; Aguerre et al. 1989; Don MacElroy and Raghavan 1991). For a complete picture of the transport across novel materials, it is necessary to take advantage of the experimental measurements recently done (Hanikel et al. 2019) and to develop a theoretical approach that fully accounts for such results to provide a realistic picture of the transport properties. Moreover, such a framework needs to be coupled to the self-driven flow produced by natural convection.

The aim of this work is to formulate a theoretical framework to evaluate the viability of continuous water harvesting systems. For this, it is proposed a theoretical model that considers the specific properties of four recently developed materials, namely MOF-303, Al-Fumarate, SAPO-34 and Zeolite 13X. Each material is packed in a rectangular bed of low thickness put in contact with air at the largest area faces, such as one of the rectangular faces is heated, whereas the opposite face is kept at room temperature. The material allows for the formation of spontaneous natural convection, which produces an effective mass transfer between both air phases, the hot air current is water-enriched and ready for recovery according to a device that accounts for some features from the US patent number US4377398 (Bennett 1979).

In sum, this work provides theoretical insights toward the enhancement of water harvesting systems by employment of complex operation of the novel materials recently developed. Nonetheless, this work is limited by the availability of dynamic desorption data; in consequence, in this work it is accounted for both the asymptotic diluted diffusion coefficient, as well as the thermodynamic correction given by the equilibrium adsorption/desorption isotherm. If more detailed information is provided at the dynamic desorption at short times, the model presented in this work can be improved further by modern techniques that combine theoretical and experimental analysis of dynamic desorption data, such as zero-length column chromatography (Vargas-Bustamante et al. 2022). Those techniques have been developed to compute in full detail the nonFickean nature of diffusion coefficient in this type of micro- and nano-porous materials.

In Sect. 2, details about the physical system under study are given along with the main physical-chemical aspects and considerations of the model, with special emphasis on the

physical and mathematical aspects required to couple the transport in each air phase with the solid adsorbent. Also, the specific properties of each material are included in the model. In Sect. 3, the solution of the model is given by numerical means and a description of the main physical and operational parameters that impact on the performance of a specific experimental setting are given. Finally, a discussion on the role of each physical parameter in the local profiles of velocity and densities is provided in Sect. 4, in order to understand the main physical mechanisms that govern water transport according to our simulations. Such discussion encompasses the most significant aspects that need to be accounted for an experimental setting intended for water harvesting in continuous flow systems.

2 Model

The system under study consists of a rectangular bed made of a porous solid material (namely MOF-303, Al-Fumarate, SAPO-34 or Zeolite 13X) placed in an inclined device, according to Fig. 1. The top face of the bed is in contact with air and its surface temperature is controlled and kept homogeneous. In addition, the bottom face of the prism is in contact with air and its surface is kept at room temperature. In all this theoretical work, it is considered that a steady state has been reached for all the temperature, air flow velocity and water density profiles.

2.1 Modeling the Solid Phase

In this work, it is considered that the thermal energy transport across the solid material is dominated by thermal conduction, and the energy conservation is given by

$$k_s \frac{\partial^2 T}{\partial y^2} = 0, \tag{1}$$

subject to the temperature imposed at the two opposite faces of the solid material, as follows:

$$T\left(x, y = -\tfrac{d}{2}\right) = T_0, \quad T\left(x, y = \tfrac{d}{2}\right) = T_1, \tag{2}$$

where d stands for bed thickness, whereas T_0 corresponds to the room temperature, whose value is sufficiently low to promote the adsorption of water from the surrounding air by the surface of the solid material. Accordingly, T_1 corresponds to a high temperature induced on the opposite surface, where water is desorbed from the solid phase to the air. Of course, there is a complex energetic process ocurring at the air-solid interphases; nonetheless, this work departs from the assumption that such a balance is experimentally controlled to guarantee a constant temperature at each surface, as stated in Eq. (2). The overall water mass transport can be divided into three processes: the water adsorption from the cold air phase by the low temperature solid surface at $y = -\frac{d}{2}$; the diffusion of water from the low temperature surface to the high temperature surface through the adsorbent bed; and the desorption of water from the hot solid surface at $y = \frac{d}{2}$ to the hot air phase.

The temperature profile inside the solid material is given by the solution of differential equation (1) subject to the boundary conditions (2), as follows:

$$T(y) = T_0 + \left(T_1 - T_0\right)\left(\frac{y + \frac{d}{2}}{d}\right). \tag{3}$$

The temperature profile $T(y)$ given by Eq. (3) must be included in the water mass transport. The solid phase made of porous material is modeled as a non-Fickean diffusive material, since convective mass transport is negligible given the small pore size and the negligible pressure difference across the solid material. In addition, because of the long aspect ratio of the material, the diffusion along x-direction is negligible compared to the diffusion along y-direction. Then, the non-Fickean behavior is directly incorporated from the experimental data reported by Hanikel et al. (2019), as explained next. First, the temperature- and concentration-dependent diffusion coefficient is given by

$$D_{\mathrm{w,s}}\left(c_{\mathrm{w}}^{\mathrm{s}}, T\right) = D_0(T)\left[\frac{\partial \ln(p_{\mathrm{w}}^{\mathrm{s}})}{\partial \ln(c_{\mathrm{w}}^{\mathrm{s}})}\right]_T = D_0(T)\frac{c_{\mathrm{w}}^{\mathrm{s}}}{p_{\mathrm{w}}^{\mathrm{s}}(c_{\mathrm{w}}^{\mathrm{s}}, T)}\left[\frac{\partial p_{\mathrm{w}}^{\mathrm{s}}\left(c_{\mathrm{w}}^{\mathrm{s}}, T\right)}{\partial c_{\mathrm{w}}^{\mathrm{s}}}\right]_T. \tag{4}$$

The computation of the infinite dilution diffusion coefficient D_0 is estimated by fitting the experimental data on dynamic desorption reported by Hanikel et al. (2019), using the long-time method typically employed in the literature. To do so, an average particle size was determined from SEM images reported in the same work. The temperature dependence of D_0 is well-represented by an Arrhenius-like function, of the form $D_0(T) = A\, e^{-\frac{B}{T}}$, where the coefficients A and B for each material are presented in Supplementary Material. Then, the adsorption isotherm $p_{\mathrm{w}}^{\mathrm{s}} = p_{\mathrm{w}}^{\mathrm{s}}(c_{\mathrm{w}}^{\mathrm{s}}, T)$ is computed by fitting experimental data reported by Hanikel et al. (2019) to a multi-centered sigmoid function, that accurately describes the reported data in all the experimental range of temperature and water concentration. Details about nonlinear regression analysis are provided in Supplementary Material. With all these considerations, water mass transport is given by

$$\frac{\mathrm{d}}{\mathrm{d}y}\left\{D_0(T)\frac{c_{\mathrm{w}}^{\mathrm{s}}}{p_{\mathrm{w}}^{\mathrm{s}}(c_{\mathrm{w}}^{\mathrm{s}}, T)}\left[\frac{\partial p_{\mathrm{w}}^{\mathrm{s}}\left(c_{\mathrm{w}}^{\mathrm{s}}, T\right)}{\partial c_{\mathrm{w}}^{\mathrm{s}}}\right]_T \frac{\mathrm{d}c_{\mathrm{w}}^{\mathrm{s}}}{\mathrm{d}y}\right\} = 0, \quad -\tfrac{d}{2} \le y \le \tfrac{d}{2}. \tag{5}$$

This model assumes that the water concentration has reached equilibrium at the air/solid interfaces where the water exchange occurs. This is incorporated as boundary conditions, as follows:

$$p_{\mathrm{w}}^{\mathrm{air}}\left[\rho_{\mathrm{w}}^{\mathrm{c}}\left(y = -\tfrac{d}{2}\right), T_0\right] = p_{\mathrm{w}}^{\mathrm{s}}\left[c_{\mathrm{w}}^{\mathrm{s}}\left(y = -\tfrac{d}{2}\right), T_0\right], \tag{6}$$

$$p_{\mathrm{w}}^{\mathrm{air}}\left[\rho_{\mathrm{w}}^{\mathrm{h}}\left(y = \tfrac{d}{2}\right), T_1\right] = p_{\mathrm{w}}^{\mathrm{s}}\left[c_{\mathrm{w}}^{\mathrm{s}}\left(y = \tfrac{d}{2}\right), T_1\right], \tag{7}$$

where the pressure at the air phases, denoted by $p_{\mathrm{w}}^{\mathrm{air}}$, is computed by considering an ideal gas, as

$$p_{\mathrm{w}}^{\mathrm{air}}\left(\rho_{\mathrm{w}}^{\mathrm{c,h}}, T\right) = \frac{\rho_{\mathrm{w}}^{\mathrm{c,h}} RT}{M_{\mathrm{w}}},$$

where M_w is the molar mass of water and R stands for the universal gas constant.

The water concentration profiles can be computed by the numerical solution of Eq. (5) with the boundary conditions in Eqs. (6) and (7). However, these boundary conditions couple water concentration in the solid phase, c_w^s, with water concentration in the air phases, ρ_w^c and ρ_w^h. Therefore, the model for water transport at air phases is presented next.

2.2 Modeling the Air Phases

The model for air phases departs from the general equations for mass, energy and momentum conservation within the Boussinesq approximation (Nelson and Wood 1989; Chamkha and Khaled 2001). For the hot air phase, which receives water from the solid material, natural convection is produced by two driving forces: first, a decrease in air density caused by the increase of temperature that comes from the heated solid surface; second, an increase in air density caused by gain of water that comes from the solid phase. It is considered that convection and diffusion effects are relevant in the transport of water mass, air momentum and energy. In addition, the diffusion along the x-coordinate is much smaller than the one along y-direction (see Fig. 1). These effects are incorporated in the following equations:

Mass balance equation

$$\frac{\partial v_x^h}{\partial x} + \frac{\partial v_y^h}{\partial y} = 0, \tag{8}$$

water mass balance equation

$$\frac{\partial \rho_w^h v_x^h}{\partial x} + \frac{\partial \rho_w^h v_y^h}{\partial y} = D_{w,air} \frac{\partial^2 \rho_w^h}{\partial y^2}, \tag{9}$$

momentum balance equation

$$\begin{aligned} \rho_0 v_x^h \frac{\partial v_x^h}{\partial x} + \rho_0 v_y^h \frac{\partial v_x^h}{\partial y} = &-\frac{\partial p}{\partial x} - \rho_0 g \sin(\theta) + \mu \frac{\partial^2 v_x^h}{\partial y^2} \\ &+ \rho_0 g \sin(\theta)\, \beta \left(T^h - T_0\right) \\ &- \rho_0 g \sin(\theta)\, \beta_w \left(\rho_w^h - \rho_{w0}\right), \end{aligned} \tag{10}$$

and energy balance equation

$$\rho_0 \hat{C}_p v_x^h \frac{\partial T^h}{\partial x} + \rho_0 \hat{C}_p v_y^h \frac{\partial T^h}{\partial y} = k \frac{\partial^2 T^h}{\partial y^2}, \tag{11}$$

where the thermodynamic coefficients β and β_w are computed by rewriting the air density in terms of partial water density and temperature, considering that air obeys the ideal gas behavior, as

$$\rho(\rho_w, T) = \rho_w + \frac{M_{dry} p_{dry}}{RT}, \tag{12}$$

where M_{dry} stands for the molar mass of dry air and p_{dry} is the partial pressure of dry air. The partial pressure is considered as a constant quantity in all the calculations in this work, computed in a straightforward manner from the atmospheric pressure and the initial air

humidity. From Eq. (12), the corresponding derivatives of air density are carried out to obtain β and β_{w}, as shown below:

$$\begin{aligned}\beta &= -\frac{1}{\rho_0}\left(\frac{\partial \rho}{\partial T}\right)_{\rho_{\mathrm{w}}}\Bigg|_{T=T_0,\rho_{\mathrm{w}}=\rho_{\mathrm{w0}}} = \frac{M_{\mathrm{dry}}p_{\mathrm{dry}}}{\rho_0 R T_0^2},\\ \beta_{\mathrm{w}} &= \frac{1}{\rho_0}\left(\frac{\partial \rho}{\partial \rho_{\mathrm{w}}}\right)_{T}\Bigg|_{T=T_0,\rho_{\mathrm{w}}=\rho_{\mathrm{w0}}} = \frac{1}{\rho_0}.\end{aligned} \tag{13}$$

For the cold air phase, which transfers water to the solid material, natural convection is produced only by a decrease in air density caused by water loss. It is considered that convection and diffusion effects are relevant in the transport of water mass and air momentum. In addition, the diffusion along the x-coordinate is much smaller than the one along y-direction (see Fig. 1). These effects are incorporated in the following equations:

Mass balance equation

$$\frac{\partial v_x^{\mathrm{c}}}{\partial x} + \frac{\partial v_y^{\mathrm{c}}}{\partial y} = 0, \tag{14}$$

water mass balance equation

$$\frac{\partial \rho_{\mathrm{w}}^{\mathrm{c}} v_x^{\mathrm{c}}}{\partial x} + \frac{\partial \rho_{\mathrm{w}}^{\mathrm{c}} v_y^{\mathrm{c}}}{\partial y} = D_{\mathrm{w,air}}\frac{\partial^2 \rho_{\mathrm{w}}^{\mathrm{c}}}{\partial y^2}, \tag{15}$$

and momentum balance equation

$$\rho_0 v_x^{\mathrm{c}}\frac{\partial v_x^{\mathrm{c}}}{\partial x} + \rho_0 v_y^{\mathrm{c}}\frac{\partial v_x^{\mathrm{c}}}{\partial y} = -\frac{\partial p}{\partial x} - \rho_0 g\sin(\theta) + \mu\frac{\partial^2 v_x^{\mathrm{c}}}{\partial y^2} - \rho_0 g\sin(\theta)\,\beta_{\mathrm{w}}\left(\rho_{\mathrm{w}}^{\mathrm{c}} - \rho_{\mathrm{w0}}\right). \tag{16}$$

This work deals with air in a solid material of moderate size with a small confinement size, involving a moderate change in temperature. The material also has a very large Grashof number, while the Reynolds number is very small. Both parameters allow neglecting the forced convection effects, and the pressure profile along the system will be approximately equal to the hydrostatic pressure. This assumption is given by

$$\frac{\partial p}{\partial x} = -\rho_0 g\sin(\theta). \tag{17}$$

Substituting the consideration of pressure in Eq. (17) into momentum balance, given by Eqs. (10) and (16) leads to the following simplified expressions:

$$\begin{aligned}\rho_0 v_x^{\mathrm{h}}\frac{\partial v_x^{\mathrm{h}}}{\partial x} + \rho_0 v_y^{\mathrm{h}}\frac{\partial v_x^{\mathrm{h}}}{\partial y} = \mu\frac{\partial^2 v_x^{\mathrm{h}}}{\partial y^2} &+ \rho_0 g\sin(\theta)\,\beta\left(T^{\mathrm{h}} - T_0\right)\\ &- \rho_0 g\sin(\theta)\,\beta_{\mathrm{w}}\left(\rho_{\mathrm{w}}^{\mathrm{h}} - \rho_{\mathrm{w0}}\right),\end{aligned} \tag{18}$$

$$\rho_0 v_x^{\mathrm{c}}\frac{\partial v_x^{\mathrm{c}}}{\partial x} + \rho_0 v_y^{\mathrm{c}}\frac{\partial v_x^{\mathrm{c}}}{\partial y} = \mu\frac{\partial^2 v_x^{\mathrm{c}}}{\partial y^2} - \rho_0 g\sin(\theta)\,\beta_{\mathrm{w}}\left(\rho_{\mathrm{w}}^{\mathrm{c}} - \rho_{\mathrm{w0}}\right). \tag{19}$$

Thus, the solution of the model for hot air phase, given in Eqs. (8), (9), (18) and (11), needs to consider the following boundary conditions:

$$
\begin{aligned}
&v_x^{\mathrm{h}}(x=0,y)=0, \quad v_x^{\mathrm{h}}(x,y=\tfrac{d}{2})=0, \quad v_x^{\mathrm{h}}(x,y=\infty)=0,\\
&v_y^{\mathrm{h}}(x,y=\tfrac{d}{2})=0,\\
&T^{\mathrm{h}}(x=0,y)=T_0, \quad T^{\mathrm{h}}\left(x,y=\tfrac{d}{2}\right)=T_1, \quad T^{\mathrm{h}}(x,y=\infty)=T_0,\\
&-D_{\mathrm{w,air}}\frac{\partial \rho_{\mathrm{w}}^{\mathrm{h}}}{\partial y}\left(x,y=\tfrac{d}{2}\right)=-D_{\mathrm{w,s}}\left(c_{\mathrm{w}}^{\mathrm{s}}\left(x,y=\tfrac{d}{2}\right),T_1\right)\frac{\partial \rho_{\mathrm{w}}^{\mathrm{s}}}{\partial y}\left(x,y=\tfrac{d}{2}\right),\\
&\rho_{\mathrm{w}}^{\mathrm{h}}(x=0,y)=\rho_{\mathrm{w0}}, \quad \rho_{\mathrm{w}}^{\mathrm{h}}(x,y=\infty)=\rho_{\mathrm{w0}}.
\end{aligned}
\tag{20}
$$

Finally, the solution of the model for cold air phase, given in Eqs. (14), (15) and (19), needs to consider the following boundary conditions:

$$
\begin{aligned}
&v_x^{\mathrm{c}}(x=0,y)=0, \quad v_x^{\mathrm{c}}\left(x,y=-\tfrac{d}{2}\right)=0, \quad v_x^{\mathrm{c}}(x,y=-\infty)=0,\\
&v_y^{\mathrm{c}}\left(x,y=-\tfrac{d}{2}\right)=0,\\
&-D_{\mathrm{w,air}}\frac{\partial \rho_{\mathrm{w}}^{\mathrm{c}}}{\partial y}\left(x,y=-\tfrac{d}{2}\right)=-D_{\mathrm{w,s}}\left(c_{\mathrm{w}}^{\mathrm{s}}\left(x,y=-\tfrac{d}{2}\right),T_0\right)\frac{\partial \rho_{\mathrm{w}}^{\mathrm{s}}}{\partial y}\left(x,y=-\tfrac{d}{2}\right),\\
&\rho_{\mathrm{w}}^{\mathrm{c}}(x=0,y)=\rho_{w0}, \quad \rho_{\mathrm{w}}^{\mathrm{c}}(x,y=-\infty)=\rho_{w0}.
\end{aligned}
\tag{21}
$$

The presented model is completely consistent with the classical treatment of natural convection problems in inclined plates, given in the literature (Eckertf and Carlson 1961; Fujii and Imura 1972; Sparrow and Azevedo 1985; Van and Lin 1990; Chamkha and Khaled 2001; Azizi et al. 2007; Singh and Singh 2018; Bodoia and Osterle 1962; Aung et al. 1972; Nelson and Wood 1989). In addition, all the equations are coupled, so a robust numerical scheme for solving them simultaneously has been carried out. The results of these computations are presented in the following sections.

3 Results

To know how much water is transferred from the cold air flow to the hot air flow, the solution of the aforementioned system of coupled transport equations is computed. To do so, values for the initial geometrical and physical parameters of the system are provided. Then, flow velocities, temperature and concentration profiles are computed. Finally, useful auxiliary quantities are computed from spatial profiles to clearly illustrate the impact and relevance of these results for water exchange. The logical flow of our computations is summarized in Fig. 2.

The first parameter that is defined in our computations is the air mass flow rate generated by natural convection at both the hot and cold air phases, $Q_{\mathrm{air}}^{\mathrm{h}}$ and $Q_{\mathrm{air}}^{\mathrm{c}}$, respectively. Also, the partial mass flow rate of water inside each air current is computed as $Q_{\mathrm{w}}^{\mathrm{h}}$ and $Q_{\mathrm{w}}^{\mathrm{c}}$. These quantities are defined as follows:

Air mass flow rate:

$$
Q_{\mathrm{air}}^{\mathrm{h,c}} \equiv W \int_0^{\infty} \rho_0 \, v^{\mathrm{h,c}}(x=L,y)\,\mathrm{d}y. \tag{22}
$$

Water mass flow rate:

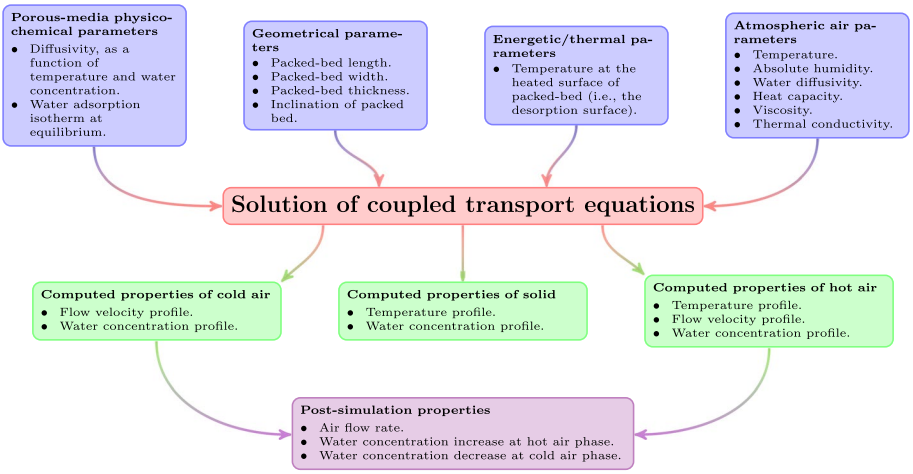

Fig. 2 Global view of the main input and output parameters involved in the sequence of computations

$$Q_{\mathrm{w}}^{\mathrm{h,c}} \equiv W \int_0^{\infty} \rho_w^{\mathrm{h,c}}(x = L, y) v^{\mathrm{h,c}}(x = L, y)\, \mathrm{d}y. \tag{23}$$

where W stands for the bed width.

The effect of the main physical parameters in water transport is described in detail, in order to understand the underlying physics and to establish perspectives for the better use of this proposed experimental setting in the future.

3.1 General Trends of Natural Convection

Figure 3 shows the effect of the entire system inclination angle and the hot solid surface temperature in water flow rate at the hot air phase. Both temperature and inclination angle have a positive correlation with flow rates. The term $\rho_0 g \sin(\theta)\beta\left(T - T_0\right)$ in equation (18) can help us to explain this correlation. It increases with increasing environment temperature (T) and angle (θ) from values greater than 0° to 90°. In addition, this term plays the role of the main driving force in the momentum equation (18). Next term, $\rho_0 g \sin(\theta)\beta_{\mathrm{w}}\left(\rho_{\mathrm{w}}^{\mathrm{h}} - \rho_{\mathrm{w0}}\right)$, is also a driving force. Nonetheless, such a concentration-driven natural convection is much smaller than the temperature-driven one. The rest of the terms in Eq. (18) respond to driving forces. All of them cause a change in the air velocity field and, consequently, in the flow rates [see Eqs. (22) and (23)]. An increase in temperature of hot surface $\left(T_1\right)$ causes a heat exchange with the medium that increases T in the driving force term and, consequently, an increase in the flow rate as shown in Fig. 3. The air mass flow rate dependence with θ is more evident since the aforementioned driving force increases with θ.

There are no significant differences between the curves shown in Fig. 3 for the different materials under study. This is due to the fact that the driving force term in Eq. (18) does not depend on the properties of the solid, but on the properties of the air. In contrast, the properties of the solid play an important role in the water adsorption process, mostly governed by Eq. (9), as will be discussed in the next section.

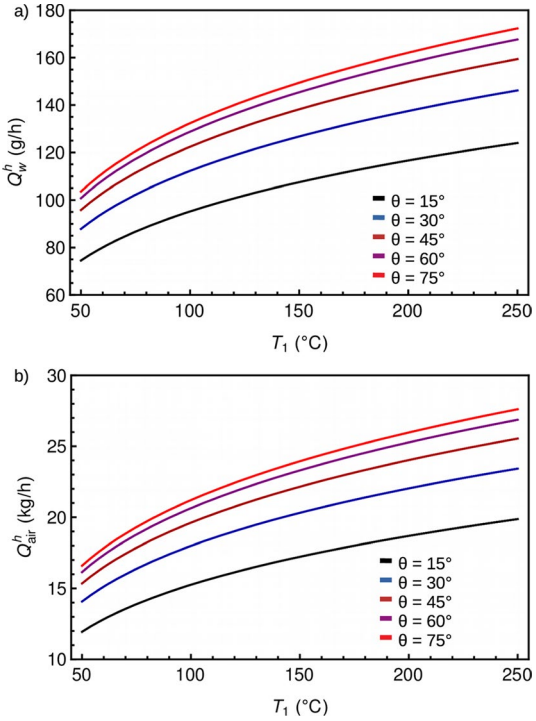

Fig. 3 Effect of temperature and inclination in water flow rate at the hot air phase. A solid phase thickness of 1 cm, solid phase length of 0.5 m and width of 1 m is considered. Also, water mole fraction at the atmosphere is set to 0.01 in these computations

3.2 Role of Thermodynamic Properties of Solid Material

In addition to the generalities described in previous subsection, other quantitative results of our model differ from one solid material to the other. As shown in Fig. 4, each solid material has different thermodynamic and transport properties and, therefore, the water uptake and release achieved differs among materials. This effect is quite small for the hot air phase in terms of flow rate. However, this contribution is the most relevant for the cold phase, where no thermal conduction occurs, so natural convection induced by water exchange is the main driving force.

Besides the magnitude of flow rates at the cold air phase, the properties of each solid material also have an impact on the change of concentration produced at each air phase. The relative change of water concentration at the hot or cold air phase, denoted by χ_h or χ_c, respectively, is defined as

$$\chi_h(y) \equiv \frac{\rho_w^h(x = L, y) - \rho_{w0}}{\rho_{w0}} \tag{24}$$

$$\chi_c(y) \equiv \frac{\rho_{w0} - \rho_w^c(x = L, y)}{\rho_{w0}}. \tag{25}$$

This is, in turn, the most important parameter in water harvesting. On the one hand, a value of χ_c very close to zero implies that all the water has been quantitatively extracted from the cold air current. On the other hand, it is very important to achieve a significant increase

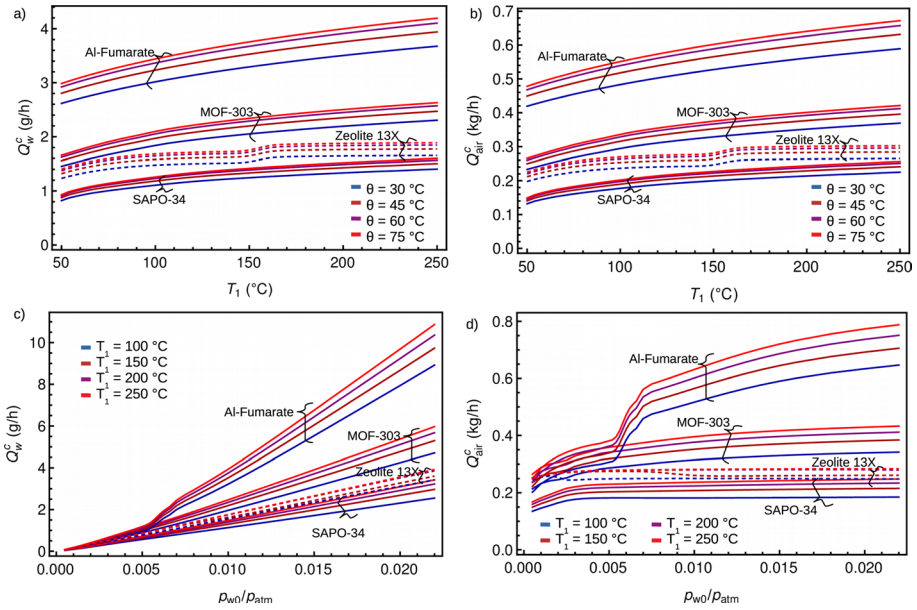

Fig. 4 Effect of temperature and atmospheric humidity in water flow rate at the cold air phase. **a** Effect of temperature in air mass flow rate at the cold phase. **b** Effect of temperature in water mass flow rate at the cold phase. **c** Effect of atmospheric absolute humidity in air mass flow rate at the cold phase. **d** Effect of atmospheric absolute humidity in water mass flow rate at the cold phase. In **a, b** water mole fraction at the atmosphere is set to $p_w/p_{atm} = 0.01$. In **c, d** bed inclination is set to $\theta = 45°$. In all cases, a solid phase thickness of 1 cm, solid phase length of 0.5 m and width of 1 m is considered

of water concentration at the hot air phase in order to use this air current subsequently in water harvesting by condensation with a relatively small energetic cost. So, a value of χ_h much higher than one is desirable. For example, in order to reach an absolute humidity of 30% in an environment with atmospheric absolute humidity of 1%, it would be necessary to achieve $\chi_h \geq 29$. For these reasons, the relative change of water concentration is the magnitude on which the rest of this work will focus.

From a physicochemical point of view, the relative change of water concentration depends on all the transport and equilibrium properties of the solid phase. These properties depend entirely on the temperature and the concentration of water in the surrounding air, as shown in the functional dependence of water/solid diffusivity and adsorption/desorption isotherm in Eqs. (4), (6) and (7). Thus, the effects of temperature at the heated solid surface and atmospheric water concentration are shown in Fig. 5. It is noticeable that one of the molecular sieves, Al-Fumarate, outstands as the most efficient for water exchange in a wide range of temperatures and atmospheric humidity. MOF-303 is the second most efficient material, and only at very small water humidity it is found a condition where MOF-303 outstands Al-Fumarate. It is also observed that all the materials exhibit the same qualitative behavior: the larger the temperature at the heated solid surface, the more efficient water exchange is. It should be noted that three of the porous materials (SAPO-34, MOF-303 and Zeolite 13X) follow the same behavior with atmospheric humidity: a moderate monotonical decrease in water exchange efficiency is observed for larger atmospheric humidities. In contrast, Al-Fumarate obeys a non-monotonical behavior with atmospheric humidity,

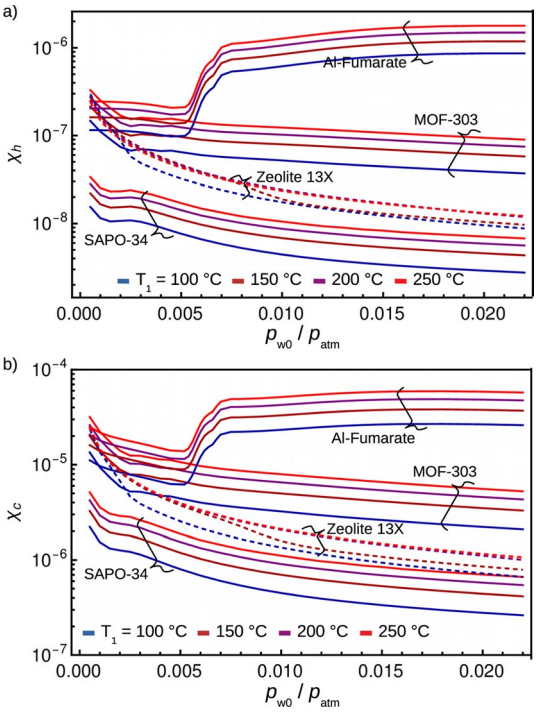

Fig. 5 Effect of the atmospheric air humidity in water transport **a** at the hot air phase and **b** at the cold air phase. A solid phase thickness of 1 cm, solid phase length of 0.5 m and width of 1 m is considered. In both panels, the vertical axes depict the coefficients χ_h and χ_c evaluated at $y = \frac{d}{2}$, i.e. at the air in contact with the heated solid surface

where a maximum efficiency in water exchange occurs at intermediate values of absolute humidity.

The fact that χ_h is roughly a decreasing function of atmospheric humidity is of great relevance, because it demonstrates that water exchange is not limited by humidity in continuous water harvesting, as in batch scheme. In turn, continuous flow systems do not exhibit a significant decrease in performance for very low humidities (below 1% of absolute humidity), compared to the higher humidity conditions. This trend is kept for MOF-303, SAPO-34 and Zeolite 13X. The only exception is found for Al-Fumarate, where there is a clear improvement of water exchange at the hot air phase for humidities from 1 to 3%.

3.3 Role of Geometrical Properties of Packed Bed

Relative changes in water concentration are small in both the hot (χ_h) and cold (χ_c) surfaces. This suggests that the water exchange between the cold and hot air streams is inefficient in all cases. In consequence, it is desirable to explore other dimensions and aspect ratio between the geometrical parameters of the packed bed, in an attempt to find characteristics that may increase the performance of these materials for water exchange in continuous flow.

The effect of packed-bed thickness and the aspect ratio between bed length and width is summarized in Fig. 6. It is observed that the optimal size arrangement of the rectangular packed bed requires using a bed as thin as possible and as long as possible. Of course, this result only comes from a theoretical point of view, an experimental array will provide another type of limitations and restrictions on the aspect ratio of a packed bed. An example

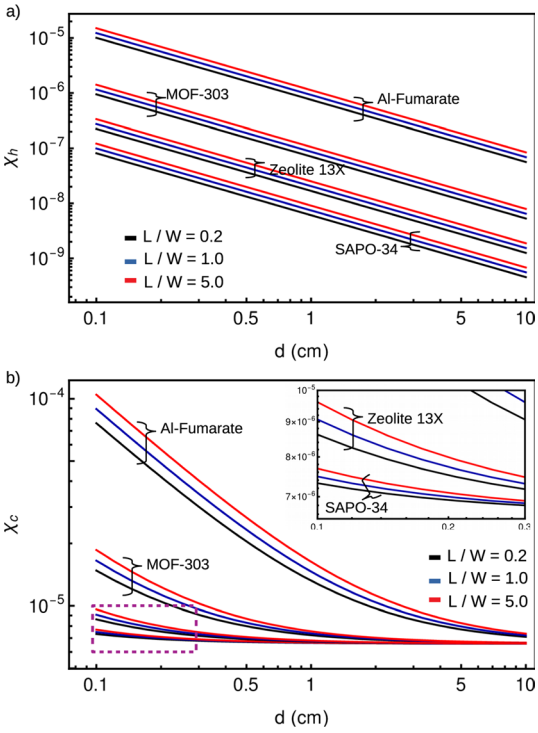

Fig. 6 Effect of the bed thickness and aspect ratio in water transport at **a** the hot air phase and **b** the cold air phase. A temperature of 150 °C at the hot solid surface is considered, and a constant packed bed volume of 5 L. In both panels, the vertical axes depict the coefficients χ_h and χ_c evaluated at $y = \frac{d}{2}$, i.e., at the air in contact with the heated solid surface

of this is the thickness d, which can only be reduced as long as the heat transfer is well-controlled and does not significantly interfere with the temperature gradient kept between the hot and cold surfaces of the solid.

4 Discussion

This work is focused on the search for physical and operational conditions where the water exchange could be enhanced in this device. As detailed in previous sections, this could be carried out whether by modifying the aspect ratio of packed bed, or by choosing an appropriate temperature at the hot solid surface. However, in all the cases explored, the relative change in water concentration is not sufficient for the purpose of water harvesting in relevant applications, since the increase in water concentration is still very low. For this reason, it is necessary to go further within the model developed here, and exploit theoretically the possibility of tuning some properties of the solid materials in order to find out which of their properties is the key factor in achieving high change in water concentration at air phases, which is the very purpose of the studied device.

4.1 Understanding Water Transport Across the Solid Phase

This study has indicated that the selected porous materials can be ordered according to their performance for water exchange as: Al-Fumarate, MOF-303, Zeolite 13X and, SAPO-34. This trend remains unchanged in most of the physical conditions explored. This is

surprising because, for different temperatures and water concentrations, the properties of these materials are completely different from one another, and still, their performance does not change that much, so each material still follows this well-established order. This could mean that there is one key property which is completely different from one system to the other, probably by orders of magnitude, such that the global performance of each material is dictated mostly by the key property.

In order to determine the key property of water exchange, it is useful to take a deeper insight in the transport process that occurs across each of the solid materials. This is summarized in Fig. 7. It is clear that there is a positive correlation between the logarithmic-average of diffusivity of water across the porous media, denoted by $D_{\mathrm{w,s}}^{\mathrm{ave}}$ and the amount of water transferred to the hot air phase, given by Fig. 7. This is understandable, from a physical point of view, as a very low diffusivity leads to low water mass flux across the material, compared to the convective mass flux that occurs by natural convection at each phase. In simple terms, very low diffusivities cause that the convective flow, tending to keep the water within each air phase, dominates over the water exchange between phases.

4.2 Impact of Diffusivity: Predicting Conditions for an Enhanced Water Harvesting

Considering our results on the role of diffusivity as the bottleneck of water harvesting, it is very useful to exploit the theoretical model presented in this work in order to predict how much larger the diffusivities should be and to make this proposed device affordable for its applications. This concept is tested in Fig. 8. In all cases, it is observed that an increase in diffusivity has a direct impact on the water exchange, both in cold and hot air phases. Nonetheless, it is reached an asymptotic point where almost all the water has been removed from the cold air phase in the proximities with the solid material. This is achieved by MOF-303 and Al-Fumarate, when diffusivity is enhanced by a factor of 10^7. For larger diffusivities, the water exchange increases only marginally. This is understood in terms of the large difference in flow rates at cold and hot air phases, observed

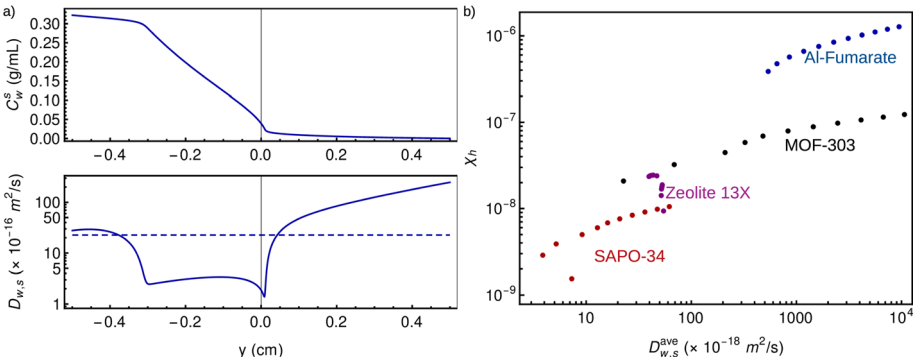

Fig. 7 **a** Water concentration and diffusion coefficient profiles across the solid phase for Al-Fumarate considering $T_1 = 150\,^{\circ}\mathrm{C}$. In particular, dashed lines show the log-average value of diffusion coefficient, $D_{\mathrm{w,s}}^{\mathrm{ave}}$. **b** Summary of computation of average diffusion coefficient and increase of water concentration at hot air phase, χ_{h}, for different temperatures and solid materials. A clear positive relation between diffusion coefficient and increase of water concentration is observed. In all the computations of (**a**), the profiles are computed considering $x = L$. In all the computations of (**b**), χ_{h} is computed at $y = \frac{d}{2}$, right next to the heated surface

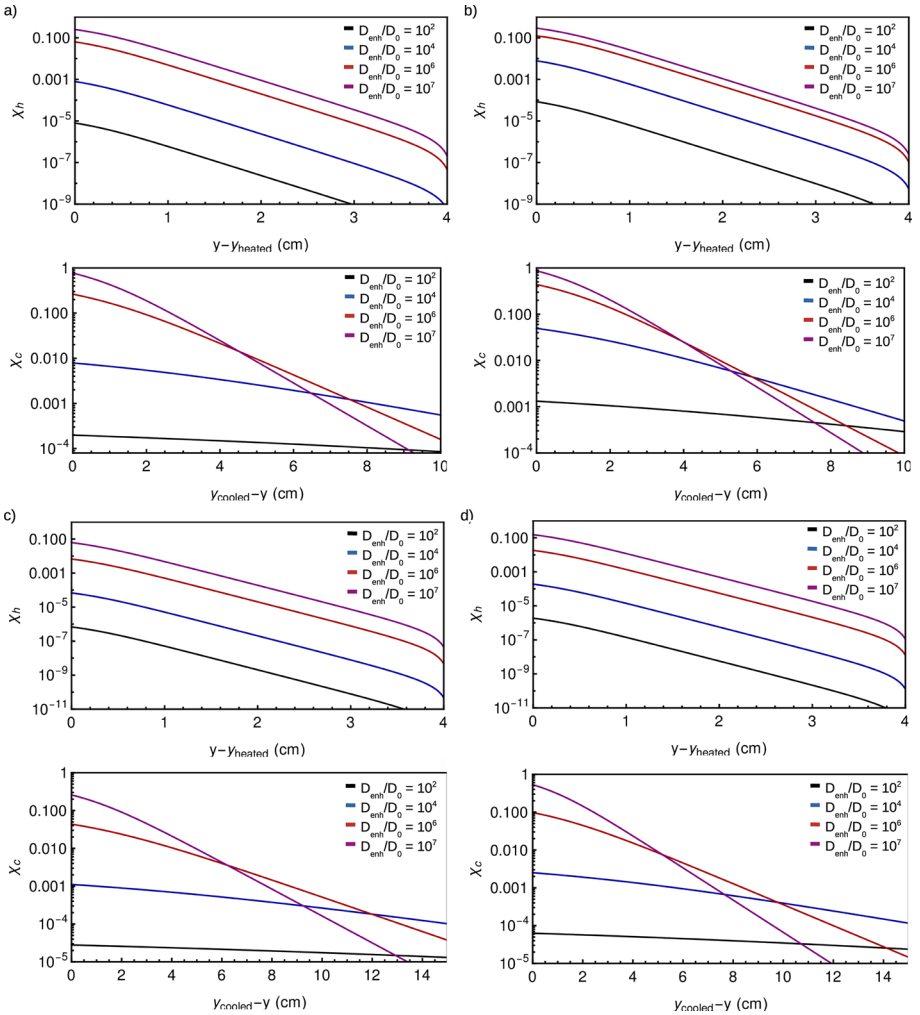

Fig. 8 Effect of an enhanced diffusivity on the water concentration profile at air phases for **a** MOF-303, **b** Al-Fumarate, **c** SAPO-34 and **d** Zeolite 13X. For each material, top panel depicts the spatial profile for hot air phase, whereas bottom panel depicts the spatial profile for cold air phase. All the profiles are computed considering $x = L, T_1 = 150\,^{\circ}\mathrm{C}$ and $p_w/p_{atm} = 0.01$

by comparison of Figs. 3 and 4. This means that the cold phase provides a low income of water to be taken by the solid phase and release towards the hot air current, because the temperature-induced natural convection in hot air current is larger than the water concentration-induced natural convection in the cold air current.

In simple terms, the results of Fig. 8 exhibit that the maximal efficiency of this device would be obtained for a material with a diffusivity seven orders of magnitude larger than the materials studied in this work. Moreover, in such a case, the limiting step would be the amount of water that can be provided by the cold phase, so there is an

upper bound in the efficiency of continuous flow for water harvesting powered only by natural convection.

5 Conclusion

Determining the conditions for water harvesting in continuous flow is very important for the development of alternatives to the conventional two-stages schemes. The operative advantages and the significant reduction of thermal charge and aging process deserves such efforts. In this work, it has been found that the four materials studied, namely MOF-303, Al-Fumarate, SAPO-34 and Zeolite 13X, require further exploration as, in their current form, these materials produce a moderate water exchange, insufficient for the target applications of water harvesting. Moreover, it has been encountered that the key factor responsible for the low performance of these materials is the extremely low diffusion coefficient. Even when consideration the complex dependence of diffusivity with temperature and water concentration, no conditions have been found where a significant water exchange is achieved. It would be necessary, to increase by seven orders of magnitude the diffusivity of these materials, in order to make natural convection continuous flow affordable.

This theoretical work relies on the diffusivity $D_0(T)$ that has been measured by the long-times method for a packed bed. Thus, the diffusion coefficient corresponds to the overall intra- and inter-crystalline diffusion process. This is important because the task of increasing the diffusion coefficient can be faced by different approaches, whether by finding other materials with different structure, or by post-synthesis treatment of the existing materials to increase their pore size. In this direction, the results obtained by (Qin et al. 2020; Han et al. 2022; Yao et al. 2023) suggest that the increase of diffusivity could be feasible by novel techniques already employed on metal–organic frameworks developed for other applications. For example, if it were possible to prepare a material in which the diffusivity of the water confined in the pores were close to that of bulk water, we would obtain diffusivities in the order of 10^{-9} to 10^{-8} m^2/s (Mills 1973; Easteal et al. 1989) and would be suitable for water harvesting, according to the results of this work. Nevertheless, this strategy conveys challenges since MOFs for water applications are limited by chemical stability against hydrolysis reactions.

It is necessary to carry out subsequent studies to develop more detailed models, focused on specific considerations that deserve further improvement. The influence of equilibrium adsorption/desorption isotherm has been completely accounted for, both in the air-solid interface and within the porous media. This is possible because our approach relies on the extensive data acquired for these novel materials in experiments under equilibrium conditions. However, more experiments on the desorption process at short times are necessary for a better modeling of the diffusion coefficient of molecular sieves at the moderate and high water concentration encountered near the water-capture-surface of the device.

The development of the theoretical approach proposed in this work, which takes full advantage of the experimental knowledge of material properties along with coupled multi-phase simulations, will constitute a strategy to assess the performance of materials in continuous flow processes in a fast and reliable manner, with the capability to increase or decrease the level of detail in transport phenomena, as needed for specific target applications in environmental technology. The enhancement of water harvesting by

simulation-tested operation conditions will be fundamental to create an affordable and feasible strategy to address water scarcity in desert and semidesert settlements.

Supplementary Information The online version contains supplementary material available at https://doi.org/10.1007/s11242-023-01962-0.

Acknowledgements U.T.-H. acknowledges financial support from CONACyT (Mexico) through Postdoctoral Fellowship (CVU 672448). The authors thank the financial support provided by DGAPA-UNAM through PAPIIT project IG100618.

Funding This work was supported by DGAPA-UNAM through PAPIIT project IG100618. Author U.T.-H. has received research support from CONACyT (Mexico) through Postdoctoral Fellowship (CVU 672448).

Data Availability The datasets generated during and/or analyzed during the current study are available from the corresponding author on reasonable request.

Declarations

Conflict of interest The authors have no relevant financial or non-financial interests to disclose.

Ethics Approval Not applicable.

Consent to Participate Not applicable.

Consent for Publication Not applicable.

References

Adeaga, O., Eslamian, S.: Assessment of Freshwater and Conservation in Africa, Chapter 8, pp. 119–139. Wiley, New York (2021). https://doi.org/10.1002/9781119776017.ch8

Aguerre, R.J., Suarez, C., Viollaz, P.E.: Relationship between energies of water sorption and diffusion in grains. Int. J. Food Sci. Technol. **24**(3), 317–320 (1989). https://doi.org/10.1111/j.1365-2621.1989.tb00649.x

Ash, R., Barrer, R.M., Edge, A.V., et al.: Thermo-osmosis of sorbable gases in porous media: part III. Single gases. J. Membr. Sci. **76**(1), 1–26 (1993). https://doi.org/10.1016/0376-7388(93)87001-R

Aung, W., Fletcher, L.S., Sernas, V.: Developing laminar free convection between vertical flat plates with asymmetric heating. Int. J. Heat Mass Transf. **15**(11), 2293–2308 (1972). https://doi.org/10.1016/0017-9310(72)90048-8

Azizi, Y., Benhamou, B., Galanis, N., et al.: Buoyancy effects on upward and downward laminar mixed convection heat and mass transfer in a vertical channel. Int. J. Numer. Methods Heat Fluid Flow (2007). https://doi.org/10.1108/09615530710730193

Bennett, C.E.: Heat energized vapor adsorbent pump. https://patents.google.com/patent/US4377398, US Patent 4377398 (1979)

Bodoia, J.R., Osterle, J.F.: The development of free convection between heated vertical plates. J. Heat Transf. **84**(1), 40–43 (1962). https://doi.org/10.1115/1.3684288

Chamkha, A.J., Khaled, A.R.A.: Similarity solutions for hydromagnetic simultaneous heat and mass transfer by natural convection from an inclined plate with internal heat generation or absorption. Heat Mass Transf. **37**(2), 117–123 (2001). https://doi.org/10.1007/s002310000131

Don MacElroy, J.M., Raghavan, K.: Transport of an adsorbing vapour in a model silica system. J. Chem. Soc. Faraday Trans. **87**(13), 1971–1987 (1991). https://doi.org/10.1039/FT9918701971

Easteal, A.J., Price, W.E., Woolf, L.A.: Diaphragm cell for high-temperature diffusion measurements. Tracer diffusion coefficients for water to 363 K. J. Chem. Soc. Faraday Trans. 1 **85**, 1091–1097 (1989). https://doi.org/10.1039/F19898501091

Eckertf, E.R.G., Carlson, W.O.: Natural convection in an air layer enclosed between two vertical plates with different temperatures. Int. J. Heat Mass Transf. **2**(1–2), 106–120 (1961). https://doi.org/10.1016/0017-9310(61)90019-9

Eslamian, S., Eslamian, F.A.: Handbook of Water Harvesting and Conservation. Wiley, New York (2021)

Fathieh, F., Kalmutzki, M.J., Kapustin, E.A., et al.: Practical water production from desert air. Sci. Adv. **4**(6), eaat3198 (2018). https://doi.org/10.1126/sciadv.aat3198

Fujii, T., Imura, H.: Natural-convection heat transfer from a plate with arbitrary inclination. Int. J. Heat Mass Transf. **15**(4), 755–767 (1972). https://doi.org/10.1016/0017-9310(72)90118-4

Gilliand, E.R., Baddour, R.F., Engel, H.H.: Flow of gases through porous solids under the influence of temperature gradients. AIChE J. **8**(4), 530–536 (1962). https://doi.org/10.1002/aic.690080422

Gilliland, E.R., Baddour, R.F., Perkinson, G.P., et al.: Diffusion on surfaces. I. Effect of concentration on the diffusivity of physically adsorbed gases. Ind. Eng. Chem. Fundam. **13**(2), 95–100 (1974). https://doi.org/10.1021/i160050a001

Gleick, P.H.: Water in crisis: paths to sustainable water use. Ecol. Appl. **8**(3), 571–579 (1998). https://doi.org/10.1890/1051-0761(1998)008[0571:WICPTS]2.0.CO;2

Han, X., Zhang, T., Wang, X., et al.: Hollow mesoporous atomically dispersed metal-nitrogen-carbon catalysts with enhanced diffusion for catalysis involving larger molecules. Nat. Commun. **13**(1), 2900 (2022). https://doi.org/10.1038/s41467-022-30520-3

Hanikel, N., Prévot, M.S., Fathieh, F., et al.: Rapid cycling and exceptional yield in a metal-organic framework water harvester. ACS Cent. Sci. **5**(10), 1699–1706 (2019). https://doi.org/10.1021/acscentsci.9b00745

Hanikel, N., Pei, X., Chheda, S., et al.: Evolution of water structures in metal-organic frameworks for improved atmospheric water harvesting. Science **374**(6566), 454–459 (2021). https://doi.org/10.1126/science.abj0890

Horiguchi, Y., Hudgins, R.R., Silveston, P.L.: Effect of surface heterogeneity on surface diffusion in microporous solids. Can. J. Chem. Eng. **49**(1), 76–87 (1971). https://doi.org/10.1002/cjce.5450490115

Hwang, S.T., Kammermeyer, K.: Surface diffusion in microporous media. Can. J. Chem. Eng. **44**(2), 82–89 (1966). https://doi.org/10.1002/cjce.5450440206

Kabo-Bah, A.T., Sedegah, D.D., Antwi, M., et al.: How to Increase Water Harvesting in Africa, Chapter 9, pp. 141–151. Wiley, New York (2021). https://doi.org/10.1002/9781119776017.ch9

Kalmutzki, M.J., Diercks, C.S., Yaghi, O.M.: Metal-organic frameworks for water harvesting from air. Adv. Mater. **30**(37), 1704,304 (2018). https://doi.org/10.1002/adma.201704304

Kim, H., Yang, S., Rao, S.R., et al.: Water harvesting from air with metal-organic frameworks powered by natural sunlight. Science **356**(6336), 430–434 (2017). https://doi.org/10.1126/science.aam8743

Kim, H., Rao, S.R., Kapustin, E.A., et al.: Adsorption-based atmospheric water harvesting device for arid climates. Nat. Commun. **9**(1), 1–8 (2018). https://doi.org/10.1038/s41467-018-03162-7

Kim, H., Rao, S.R., LaPotin, A., et al.: Thermodynamic analysis and optimization of adsorption-based atmospheric water harvesting. Int. J. Heat Mass Transf. **161**(120), 253 (2020). https://doi.org/10.1016/j.ijheatmasstransfer.2020.120253Get

LaPotin, A., Kim, H., Rao, S.R., et al.: Adsorption-based atmospheric water harvesting: impact of material and component properties on system-level performance. Acc. Chem. Res. **52**(6), 1588–1597 (2019). https://doi.org/10.1021/acs.accounts.9b00062

Levy, J., Eslamian, S.: Sustainable Water Harvesting and Conservation Using Multiple-Criteria Analysis, Chapter 2, pp. 15–33. Wiley, New York (2021). https://doi.org/10.1002/9781119776017.ch2

Mancuso, J.L., Hendon, C.H.: Porous crystals provide potable water from air. ACS Cent. Sci. **5**(10), 1639–1641 (2019). https://doi.org/10.1021/acscentsci.9b00910

Mills, R.: Self-diffusion in normal and heavy water in the range 1–45°. J. Phys. Chem. **77**(5), 685–688 (1973). https://doi.org/10.1021/j100624a025

Mouchaham, G., Cui, F.S., Nouar, F., et al.: Metal-organic frameworks and water:'from old enemies to friends'? Trends Chem. (2020). https://doi.org/10.1016/j.trechm.2020.09.004

Nelson, D.J., Wood, B.D.: Combined heat and mass transfer natural convection between vertical parallel plates. Int. J. Heat Mass Transf. **32**(9), 1779–1787 (1989). https://doi.org/10.1016/0017-9310(89)90059-8

Nguyen, H.L., Hanikel, N., Lyle, S.J., et al.: A porous covalent organic framework with voided square grid topology for atmospheric water harvesting. J. Am. Chem. Soc. **142**(5), 2218–2221 (2020). https://doi.org/10.1021/jacs.9b13094

Öhrström, L., Amombo Noa, F.M.: An improved water-harvesting cycle. Science **374**(6566), 402 (2021). https://doi.org/10.1126/science.abm1854

Pan, T., Yang, K., Han, Y.: Recent progress of atmospheric water harvesting using metal-organic frameworks. Chem. Res. Chin. Univ. **36**(1), 33–40 (2020). https://doi.org/10.1007/s40242-020-9093-6

Qin, Y., Han, X., Li, Y., et al.: Hollow mesoporous metal-organic frameworks with enhanced diffusion for highly efficient catalysis. ACS Catal. **10**(11), 5973–5978 (2020). https://doi.org/10.1021/acscatal.0c01432

Sakthivadivel, R., Vennila, S.: Feasibility Study of Rainwater Harvesting Systems, Chapter 1, pp. 1–13. Wiley, New York (2021). https://doi.org/10.1002/9781119776017.ch1

Singh, A.K., Singh, A.K.: Natural convection of a micropolar fluid between two vertical walls with Newtonian heating/cooling and heat source/sink. In: Applications of Fluid Dynamics, pp. 145–157. Springer. https://doi.org/10.1007/978-981-10-5329-0_10 (2018)

Sparrow, E.M., Azevedo, L.F.A.: Vertical-channel natural convection spanning between the fully-developed limit and the single-plate boundary-layer limit. Int. J. Heat Mass Transf. **28**(10), 1847–1857 (1985). https://doi.org/10.1016/0017-9310(85)90207-8

Trapani, F., Polyzoidis, A., Loebbecke, S., et al.: On the general water harvesting capability of metal-organic frameworks under well-defined climatic conditions. Microporous Mesoporous Mater. **230**, 20–24 (2016). https://doi.org/10.1016/j.micromeso.2016.04.040

Van, W.M., Lin, T.F.: Combined heat and mass transfer in natural convection between vertical parallel plates with film evaporation. Int. J. Heat Mass Transf. **33**(3), 529–541 (1990). https://doi.org/10.1016/0017-9310(90)90187-Y

Vargas-Bustamante, J., Martínez-Ortiz, P., Alvarado-Alvarado, D., et al.: Experimental setup and graphical user interface for zero-length column chromatography. Appl. Sci. (2022). https://doi.org/10.3390/app12136694

Wang, X., Lee, C.: Water-stable metal-organic frameworks for water adsorption. In: Advances in Sustainable Energy, pp. 387–416. Springer https://doi.org/10.1007/978-3-030-74406-9_14 (2021)

Xu, W., Yaghi, O.M.: Metal-organic frameworks for water harvesting from air, anywhere, anytime. ACS Cent. Sci. **6**(8), 1348–1354 (2020). https://doi.org/10.1021/acscentsci.0c00678

Yamasaki, A., Tyagi, R.K., Fouda, A., et al.: Effect of evaporation time on the pervaporation characteristics through homogeneous aromatic polyamide membranes. II. Pervaporation performances for ethanol/water mixture. J. Appl. Polym. Sci. **60**(5), 743–748 (1996).https://doi.org/10.1002/(SICI)1097-4628(19960502)60:53.0.CO;2-#

Yao, Y., Zhao, X., Chang, G., et al.: Hierarchically porous metal-organic frameworks: synthetic strategies and applications. Small Struct. **4**(1), 2200,187 (2023). https://doi.org/10.1002/sstr.202200187

Zhou, X., Lu, H., Zhao, F., et al.: Atmospheric water harvesting: a review of material and structural designs. ACS Mater. Lett. **2**(7), 671–684 (2020). https://doi.org/10.1021/acsmaterialslett.0c00130